Available online at www.sciencedirect.com
SCIENCE DIRECT®
ELSEVIER
Nuclear Instruments and Methods in Physics Research A 532 (2004) 548–561
NUCLEAR INSTRUMENTS & METHODS IN PHYSICS RESEARCH Section A
www.elsevier.com/locate/nima

The time-of-flight TOFW detector of the HARP experiment: construction and performance

M. Baldo-Ceolin[a], G. Barichello[a], F. Bobisut[a], M. Bonesini[b,*], A. De Min[b,1], A.F. Ferri[b], D. Gibin[a], A. Guglielmi[a], M. Laveder[a], A. Menegolli[a,2], M. Mezzetto[a], M. Paganoni[b], F. Paleari[b], A. Pepato[a], A. Tonazzo[b,3], M. Vascon[a]

[a]*Sezione INFN, Dipartimento di Fisica G. Galilei, Via Marzolo 8, Padova, Italy*
[b]*Sezione INFN, Dipartimento di Fisica G. Occhialini, Piazza Scienza 3, Milano, Italy*

Received 6 April 2004; accepted 19 April 2004
Available online 21 July 2004

Abstract

The construction and performance of a large area scintillator-based time-of-flight detector for the HARP experiment at CERN are reported. An intrinsic counter time resolution of ~160 ps was achieved. The precision on the time calibration and monitoring of the detector was maintained at better than 100 ps by using dedicated cosmic rays runs, a fast laser-based system and calibrations with beam particles. The detector was operated on the T9 PS beamline during 2001 and 2002. A time-of-flight resolution of ~200 ps was obtained, providing π/p discrimination at more than 3σ up to 4.0 GeV/c momentum.

Pacs: 95.55.Vj; 29.40.Mc; 42.55.Mv; 85.60.-q

Keywords: Particle detectors; Scintillation detectors; Dye lasers; Optoelectronic devices

1. Introduction

The HARP experiment [1] is devoted to the study of hadroproduction on nuclear targets for incident beam momenta between 1.5 and 15 GeV/c, an energy range of interest for atmospheric neutrinos and for the neutrino factory design [2]. Moreover, particle yields from MiniBooNE [3] and K2K [4] target replicas were measured. Its programme was carried out at CERN, on the PS T9 beamline, in 2001 and 2002. The HARP spectrometer, shown in Fig. 1, comprises different subdetectors providing track reconstruction and particle identification over the full solid angle. At large angles tracking and particle identification (PID) is given by a TPC and

*Corresponding author.
E-mail address: maurizio.bonesini@mib.infn.it (M. Bonesini).
[1]Also at Politecnico di Milano, Milano, Italy.
[2]Now at Dipartimento di Fisica Nucleare e Teorica, Pavia, Italy.
[3]Now at Departimento di Fisica E. Amaldi, Roma Tre, Italy.

0168-9002/$ - see front matter © 2004 Elsevier B.V. All rights reserved.
doi:10.1016/j.nima.2004.04.250

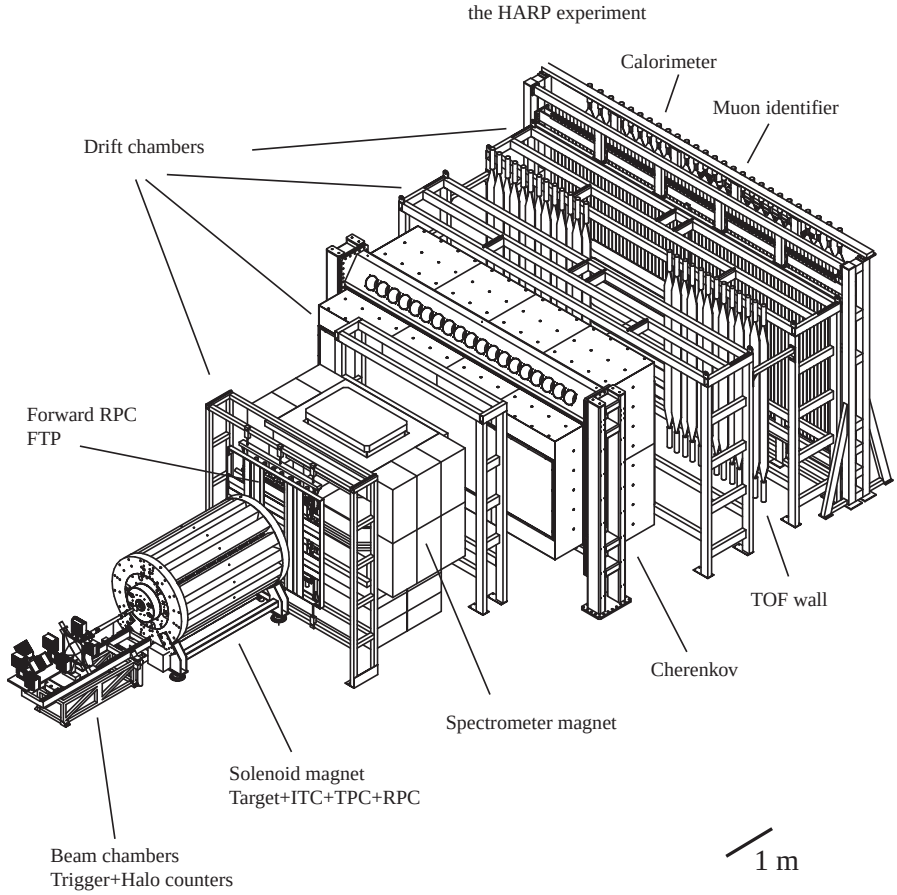

Fig. 1. Layout of the HARP spectrometer at the CERN PS. The different sub-detectors are shown. The target is inserted inside the TPC.

an array of RPC counters [5]. In the forward direction, the tracking device is a set of drift chambers [6] from the previous NOMAD experiment and particle identification is achieved by using a scintillator based time-of-flight wall (TOFW) at low momenta ($p \leqslant 3.5$ GeV/c) and a threshold Cherenkov counter at high momenta.

The requirements for the TOFW include excellent time resolution, for particle identification, and transverse segmentation to avoid particle pile-up on single counters. The system specifications call for a time resolution of about 250 ps to separate at 4σ pions from protons up to 3.5 GeV/c, on the basis of a 10 m flight path from the production target. The required time resolution is achieved by combining leading-edge time measurements (with TDC) with pulse-height information for time-walk corrections (with ADC).

2. The HARP tof wall detector

The layout of the HARP time-of-flight wall is shown in Fig. 2. The total area is $7.4 \times 2.5\,m^2$. In the left/right palisades, scintillators are 250 cm long and lie vertically, while in the central palisade scintillators are 180 cm long and lie horizontally. The scintillator counters are BC-408[4] slabs from Bicron, 2.5 cm thick and 21 cm wide. The scintillators are suitable for fast timing applications over

[4]See www.bicorn.com for more details.

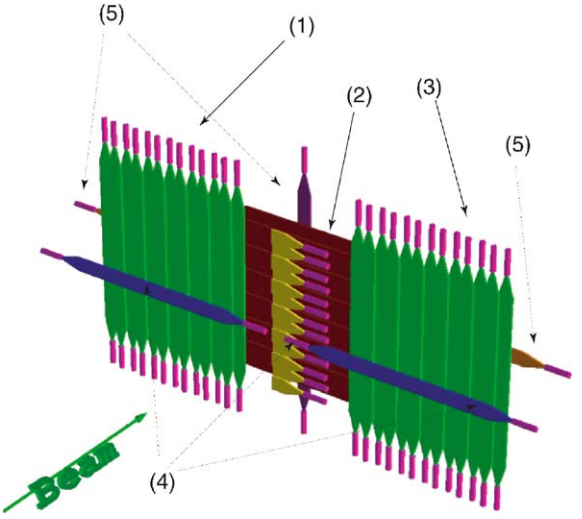

Fig. 2. Layout of the time-of-flight wall of the HARP experiment. The three palisades (1,2,3) and the additional upstream (4) and downstream counters (5), inserted for the cosmic muon calibrations, are shown.

large areas, given the good bulk attenuation length (~4 m), light yield (~10^4 photons/MeV) and fast decay time (2.1 ns). At the two ends of each scintillator slat), PMMA fish-tail light guides have been glued, tapered from the dimensions of the ends of the slabs to those of a PMMA cylinder, coupled to the photocathode of a photomultiplier tube (Philips XP2020[5]) through a disc of silicone elastomer.

The counters are wrapped in aluminium and sealed with black plastic. At the center of each counter a small prism attached to a multimode CERAM OPTEC 100/110 fiber (1 m long and 100 μm thick) allows the injection of laser light pulses to control the stability of counters and electronics (see Section 2.3 for more details).

The quantum efficiency of XP2020 photomultipliers (~26% at 401 nm) is well matched to the range of wavelengths emitted by BC-408 scintillator (λ~420 nm). The XP2020 is characterized by a fast rise time (1.5 ns) with minimal transit time spread (TTS ~250 ps), good linearity of response and can achieve a gain $G\sim 3\times 10^7$ at typical voltage of 2200 V with low background noise. The phototube is shielded from the residual magnetic fields by a cylinder of μ-metal. The high voltage was fed to the PMTs by means of an home-made passive divider installed in the sockets.

The performance of the counters was carefully studied in the construction phase and is described in Section 3.

In each palisade, adjacent counters are overlapped by 2.5 cm to ensure hermetic coverage. Moreover, the particles passing through the overlapping areas were used to cross-calibrate the counters. The mechanical system for holding PMTs and hanging the scintillation counters was carefully designed to avoid the presence of material in front of the active scintillator slabs.

Two additional sets of scintillation counters, called "calibration counters", were placed one upstream and the other downstream of the TOFW (see Fig. 2) to trigger on cosmic events. The precise position of these counters allowed the selection of cosmic muons crossing the time-of-flight wall with a zenith angle of $\theta\sim 40^\circ$. The three downstream counters (two horizontal counters with dimensions of $250\times 21\,\mathrm{cm}^2$ and one vertical counter with dimensions of $300\times 21\,\mathrm{cm}^2$) provided the reference time information for the cosmics calibration procedure and were characterized by excellent intrinsic resolution. The upstream counters consisted of two horizontal scintillators (dimensions $250\times 21\,\mathrm{cm}^2$) and of a vertical strip of 13 short scintillators with size $21\times 21\,\mathrm{cm}^2$. The upstream counters were removed during normal run operations with beam, in order to avoid the presence of extra material in front of the time-of-flight wall.

2.1. Time of flight measurement and resolution

For a particle crossing a scintillation counter i ($i=1,\ldots 39$), equipped with two photomultiplier tubes (PMT) j ($j=1,2$), at a time t_0 and at a distance x from its center, the time difference $\Delta t_{i,j}$between the STOP from the PMT j and the START from a reference counter t_s is given by

$$\Delta t_{i,j} = t_0 + \frac{L/2 \pm x}{v_{\mathrm{eff}}} - t_s + \delta_{i,j},\ j = 1,2 \qquad (1)$$

where L is the scintillator length, v_{eff} the effective light velocity in the scintillator slab

[5]See Philips Photomultipliers Data Handbook, p. 101, for more details.

($v_{\text{eff}}^{-1} \sim 6.2\,\text{ns/m}$) and $\delta_{i,j}$ include all delays (cables, PMT transit time, etc.). After correction for the delays $\delta_{i,j}$, the quantity

$$\Delta t_{+,i} = \frac{\Delta t_{i,1} + \Delta t_{i,2}}{2} = t_0 + \frac{L}{2 \cdot v_{\text{eff}}} - t_s \tag{2}$$

is independent of the impact point x along the counter i and allows the measurement of the time-of-flight (TOF), while the impact position x can be deduced from

$$\Delta t_{-,i} = \frac{\Delta t_{i,1} - \Delta t_{i,2}}{2} = \frac{x}{v_{\text{eff}}}. \tag{3}$$

The intrinsic resolution of the PMT j is given by: $\sigma_{i,j} = \sqrt{\sigma^2_{\Delta t_{i,j}} - \sigma^2_{t_s}}$ where $\sigma_{\Delta t_{i,j}}$ are the corresponding resolutions of the $\Delta t_{i,j}$ distributions. The resolution on the start time t_s can be evaluated as: $\sigma_{t_s} = \sqrt{\sigma^2_{\Delta t_{+,i}} - \sigma^2_{\Delta t_{-,i}}}$. The intrinsic resolution for the crossing time (t_0), as measured with the counter i, is given by

$$\sigma_{0,i} = \frac{1}{2}\sqrt{\sigma^2_{i,1} + \sigma^2_{i,2}} \tag{4}$$

and is equivalent to the one calculated directly from the distribution of Δt_-.

In HARP the start signal (t_s) was provided by two beam TOF counters TOFA and TOFB (2.7 and 24.1 m upstream of the target) and a Target Defining Scintillator TDS (0.2 m upstream the target). TOFA and TOFB [7], obtained from the previous NA52 experiment, were made of a plane of BC404 scintillators ($10 \times 10\,\text{cm}^2$) of 1 cm thickness, divided into eight strips of width growing from 0.8–2.0 cm at the outer edge. Every scintillator strip was matched to a PMMA lightguide and read, at both ends, by Hamamatsu H1949 PMTs. The intrinsic resolution of each counter was around 100 ps. The TDS is instead a scintillator disc of 10 mm radius and 5 mm thickness, viewed by four R1635P Hamamatsu PMTs.

2.2. Electronics readout and trigger

The analog signal from the PMTs was fed, after a 40 m long RG-213 cable, to an active splitter module. A 25% fraction of the signal was sent to the ADC line, while the full signal, after a leading edge discriminator[6] with a −38 mV threshold, was sent to the TDC line. The input impedance of the active splitters was matched to the impedance of the RG-213 cables, to reduce signal reflections. The discriminated signals were first delayed by ~220 ns using single screened twisted pair cables, then regenerated by a fast discriminator (line receiver) and finally processed by the TDCs (model CAEN V775, 32 channels, 12 bits, nominally ~35 ps/ch). The second output of the splitter was sent to a charge-integrating ADC (model CAEN V792, 12 bits, 0.1 pC/ch) after being delayed by ~240 ns.

The stability of the digital electronics was monitored by pulsing simultaneously all the channels of each discriminator with an electronic signal generated by a pulser circuit.

In addition the TOFW (counters and electronics) was globally monitored through laser pulses which are directly sent to the center of each scintillator by an optical fiber injection system a few times a day.

During data taking, a temperature excursion of $\pm 5\,^{\circ}\text{C}$ was registered in the experimental hall, while the electronics in the controfrbom was thermostatically controlled to $\pm 0.5\,^{\circ}\text{C}$, which guaranteed a time stability of a single-channel better than 50 ps (see Section 2.2.1). However, the channel to channel relative time variation, which is relevant for the time-of-flight measurement, was at a few ps level, well below the instrumental sensitivity.

The trigger pulse, which defines the START signal for the TDC and the ADC gate (with 120 ns width), was provided by four possible sources:

(1) the HARP central trigger (for physics events);
(2) a fast PIN photodiode (for the laser system);
(3) the coincidence of signals from the cosmics calibration counters (for cosmic runs);
(4) the pulser (for the monitoring of the electronics stability).

With the only exception of the local cosmic trigger, which had deliberately a standalone

[6]Model LeCroy 4413, 16 channel, modified with 330 Ω pull-down resistors, instead of the factory installed 470 Ω resistors, to improve the slew of the output signal.

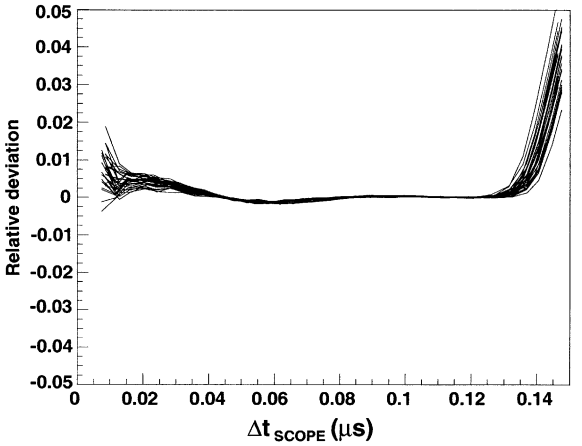

Fig. 3. Fractional deviation from a linear fit to the TDC output (Δt_{TDC}) as a function of true input Δt_{SCOPE}, for the 32 TDC CAEN V775 channels under test.

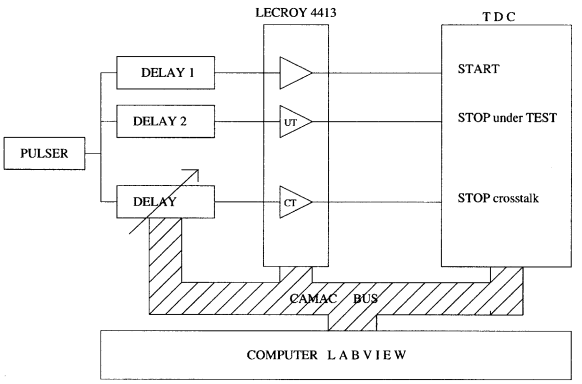

Fig. 4. Laboratory setup for discriminator and TDC cross-talk measurements.

operation mode and as a consequence was mutually exclusive with respect to the global triggers, the architecture of the system allowed mixing arbitrary in the same run any kind of trigger, keeping track of the source for offline analysis.

2.2.1. Tests of the electronics readout components

Fast timing requires cables with low signal distorsion. RG-213 cables rather than the usual RG-58 cables for fast NIM electronics were used, in order to minimize skin effect and dielectric losses. Moreover, RG-213 cables offer a better stability as a function of temperature. A single-channel time variation of 30 ppm/°C, due to thermal drift, was measured for RG-213 cables, three times better than standard RG-58 cables. In addition, a single channel time variation of 180 ppm/°C was determined for the twisted pair cables used for the passive signal delays. However, both temperature time drifts were at the level of only several ppm/°C, when considering the relative channel to channel variation.

Tests of the TDC CAEN V775 performance, as far as linearity, crosstalk and temperature variation are concerned, were performed and results are given below.

The linearity of the TDC has been measured using as a reference the time base system of a LECROY LT344 digital oscilloscope (Δt_{SCOPE}) The scope had a time accuracy of 10 ppm and a resolution in interpolation mode of 5 ps so that its global accuracy was about 4×10^{-5} of the TDC range, much better than that of the TDC (nominal LSB[7]$\sim$35 ps). A pulser circuit was used to trigger the system, to send a start signal t_0 the TDC and, after an appropriate time delay Δt, a stop signal to a single TDC channel at a time. From the fit of Δt_{TDC} vs. Δt_{SCOPE} the effective LSB was measured as $\sim$37 ps. The deviations from a linear fit of the TDC output (average Δt_{TDC}) as a function of true input Δt_{SCOPE}, for all the 32 channels of one TDC module, are shown in Fig. 3.

The measurement was repeated for all the three TDC modules used in the TOFW. The same measurements were repeated at the end of the experiment (1.5 years later) and found to be stable to better than 0.1%. The measured integral nonlinearity (INL), the maximum absolute deviation between the input Δt_{SCOPE} and the measured Δt_{TDC} referred to the Full Scale Range (FSR), was within specifications ($\pm 0.1\%$ of FSR) for $10\,\text{ns} \leqslant \Delta t_{SCOPE} \leqslant 135\,\text{ns}$.

The interchannel isolation of the time measurement, namely the dependence of any time measurement on the activity in other channels, was tested with the setup shown in Fig. 4.

To separate the TDC contribution to cross-talk from that of the discriminator, signals not over-

[7]Least significant bit.

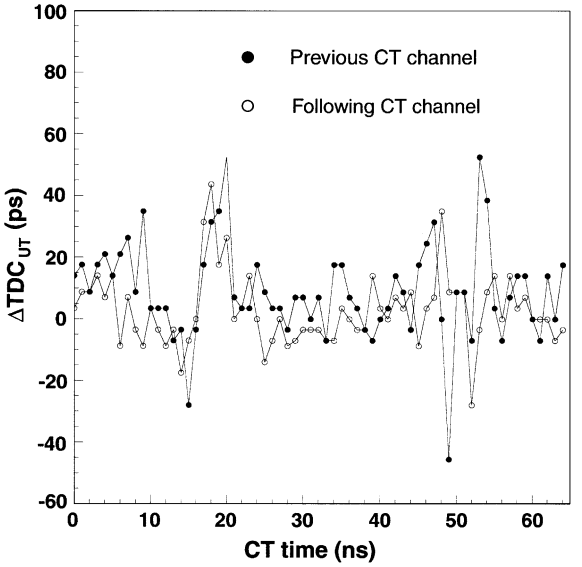

Fig. 5. Time shift in the TDC channel under test (ΔTDC_{UT}) plotted as a function of the time of two adjacent TDC firing channels (CT) which generate the crosstalk and belong to the same chip.

lapping in time were sent to well separated channels of the discriminator A pulser circuit provided, via the LeCroy 4413 discriminator, the common start signal to the TDC (START). The same pulser also simulated two different input signals to the TDC: the channel under test (UT) and the possible crosstalk generating channel (CT).

The maximum deviation in the measurement of TDC_{UT}, which represents the effect of the crosstalk between the input TDC channel (CT) and the TDC channel under test (UT), was within 50 ps for all the 32 channels (see a typical behavior in Fig. 5).

This crosstalk effect was always confined to groups of four TDC channels belonging to the same 4-channel chip, being negligible for all the combinations not belonging to a common group. These shifts of the time measurement were minimized by appropriate cabling the TDC, requiring that PMT signals coming from the same slab be fed to TDC channels located in different chips. In such a way an unavoidable crosstalk remains only in the case of PMT signals arriving in the same TDC chip within 5 ns and coming from different slabs located far away in the time-of-flight wall.

Single-channel TDC time variations of 1300 ppm/°C due to thermal drift were measured. Relative channel to channel time variation due to thermal drift, were measured to be 88 ppm/°C.

The same laboratory setup was also used to measure cross-talk between different channels on the same discriminator board. Perturbations up to 150 ps for channels belonging to the same chip were observed. Their effect was minimized by the careful cabling described above.

2.3. The laser calibration system

Drifts in the time delays (see Eq. (1)) must be included in the calibration constants $\delta_{i,j}$. Commonly the initial time alignment is obtained through cosmic rays calibration, while the time evolution of this alignment is obtained via a laser system. Previous systems include the ones used for the $N-\bar{N}$ experiment at Grenoble [8], the MARK-III experiment at SLAC [9], the CLAS system at CEBAF [10] and the TOPAZ experiment at KEK [11]. A layout of the laser calibration system of the HARP time-of-flight wall is shown in Fig. 6. For details on the construction see Ref. [12]. The laser beam was split to a fast photodiode, that gave the start for the TDC system, and was injected into a bundle of fibers that transmitted the pulse to the different scintillator channels.

For the light source of the monitoring system a custom made Nd-Yag laser[8] with passive Q-switch, active/passive mode locking and 10 Hz repetition rate was used. The infrared (IR) emission (at $\lambda = 1064$ nm) is converted into a second harmonic at 532 nm by a KD*P SHG crystal. A novel design InGaAs Metal–Semiconductor–Metal (MSM) photodetector,[9] with 30 ps rise and fall time, was used for timing the light pulse (and so to give the TDC start). To get the optimal time performance, an appropriate circuit

[8]Modified SYLP0 from Quanta systems srl, Milano, Italy: FWHM~60 ps, average enegy ~6 mJ/pulse.

[9]Hamamatsu G4176.

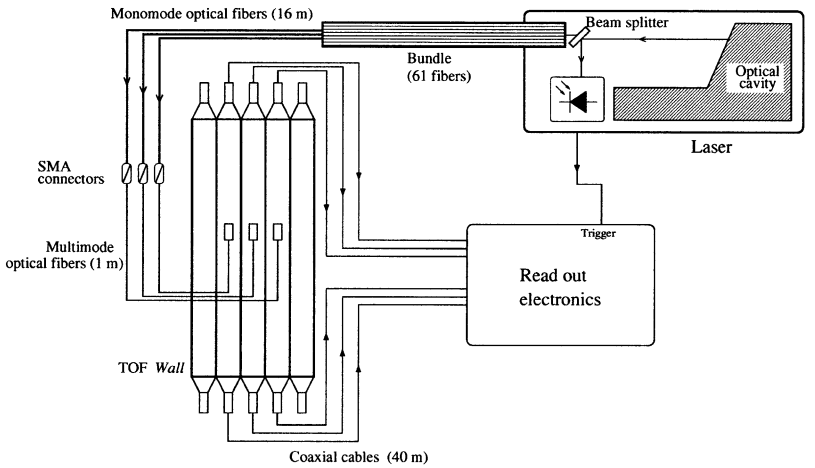

Fig. 6. Layout of the laser calibration system for the HARP TOFW. For details on the single elements see text.

connection was made with good high frequency characteristics using a very broadband ($\geqslant 10$ GHz) "bias tee"[10] to power the diode.

Due to the wide area covered by the TOFW and the requirement to have the laser source out of the experimental area for easy handling during beam data taking periods, relatively long fibers ($\sim$15 n) had to be used to inject the laser light into the scintillation counters. To avoid a big increase in the jitter of the leading edge of the injected light pulse, Corning SMF-28 IR monomode fibers (with a measured dispersion of 3.6 ps/m at 532 nm) were used.

Fibers were grouped in a bundle with a common part ($\sim$1 m) at the laser light injection and a free part going to the individual counters. At the free end of each fiber the laser signal was injected into a short (1 m long) multimode fiber[11] that ended in a small prism glued at the center of each scintillator slab. Before injection in the fiber bundle, the laser light was attenuated by a system of optical neutral filters[12] (ODC$\sim$4.5) and the laser beam spot was enlarged (to about 5 mm diameter) by a system of lenses to reduce intensity non-uniformities.

[10]Model 5550B from Picosecond Pulse Lab.
[11]CERAM OPTEC UV 100/125.
[12]Solid Glass ND filters, from Ealing Electro-optics.

3. Selection and preparation of the scintillation counters

The performance of each scintillation counter was measured in the laboratory with cosmic rays, selected by five telescopes, each made of three small scintillator counters (about $10 \times 10\,\mathrm{cm}^2$) and put at different positions along the scintillators under test.

Signals from the counters under test were split by a resistive splitter: 75% of the signal was sent to a discriminator, properly delayed and then sent to a TDC individual stop. The remaining 25% was delayed and sent to an ADC, which measured integral charge in the 120 ns gate.

Photomultiplier charge spectra were fitted to a Landau distribution, to determine the peak charge Q. The effective attenuation length was measured as $\lambda = (395 \pm 6)$ cm.

Initially, the time resolutions averaged over the five selected positions and over all counters were found to be

$$\sigma_0(L = 250\,\mathrm{cm}) = (207 \pm 4)\,\mathrm{ps}$$
$$\sigma_0(L = 180\,\mathrm{cm}) = (201 \pm 5)\,\mathrm{ps}.$$

The intrinsic PMT time resolution shows a dependence on the impact point position (see Fig. 7). As a consequence, the determination of the crossing time t_0 with the simple arithmetic mean

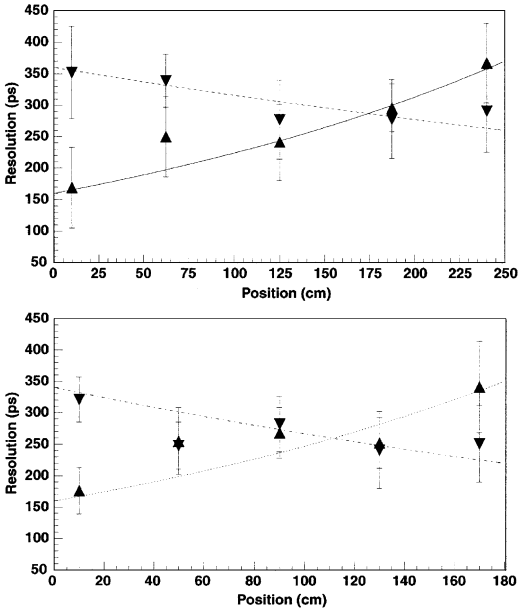

Fig. 7. Average intrinsic resolutions σ_1 (▲) σ_2 (▼) as a function of the distance from the the left PMT along L=250 cm (above) and L=180 cm (below) counters (the centers of the counters are at 125 cm and at 90 cm, respectively). The error bars show the rms of the distributions. The curves are shown to guide the eye.

(2) can be improved, if the position x of the hit along the counter is measured independently (as with the tracking system in the HARP experiment).

The intrinsic time counter resolution can be estimated with a weighted mean as

$$\sigma_0^{\mathrm{W}} = \sqrt{\left[\frac{1}{\sigma_1^2} + \frac{1}{\sigma_2^2}\right]^{-1}} \tag{5}$$

where σ_1, σ_2 are the time resolutions of the two PMTs of a scintillation slab. The averages of σ_0^{W} over the five positions were:

$$\sigma_0^{\mathrm{W}}(L = 250\,\mathrm{cm}) = (190 \pm 4)\,\mathrm{ps}$$
$$\sigma_0^{\mathrm{W}}(L = 180\,\mathrm{cm}) = (181 \pm 5)\,\mathrm{ps}$$

showing a small improvements over previous results.

The adoption of leading edge discriminators introduces a dependence of the discrimination times on the collected charge *A (time walk)*, that affects the intrinsic time resolution. The corresponding correction terms to the measured times Δt_i were parameterized by the formula [15]:

$$\delta t_i = W\left(\frac{1}{\sqrt{A_0}} - \frac{1}{\sqrt{A}}\right) \tag{6}$$

where A_0 is the peak value of the charge distribution and W is the walk parameter, to be determined experimentally. The resulting distribution of W had an average value $\sim$11.4 ns pC$^{1/2}$. After the time-walk corrections (Fig. 8) the resolutions averaged over the five telescopes for the two counter lengths are:

$$\sigma_0^{\mathrm{W}}(L = 250\,\mathrm{cm}) = (159 \pm 5)\,\mathrm{ps}$$
$$\sigma_0^{\mathrm{W}}(L = 180\,\mathrm{cm}) = (147 \pm 9)\,\mathrm{ps}.$$

This corresponds to a resolution of $\sim$3 cm on the reconstructed position along the counter by the TOFW itself.

The time resolution of the counters was also measured with the calibration laser system. Appropriate time walk corrections (see Section 4.2) were applied and ADC signals with averages compatible with a minimum ionizing particle (m.i.p) were selected. However, some care had to be taken in the comparisons, due to the different mechanisms involved in the light generation and the different wavelengths involved (532 nm for the laser light with respect to 420 nm for the scintillation emitted light). The time resolution can be evaluated by plotting the quantity Δt_- for each slab, as determined with dedicated laser runs. The average intrinsic resolutions for all the TOFW counters are:

$$\sigma_L(L = 250\,\mathrm{cm}) = (160 \pm 8)\,\mathrm{ps}$$
$$\sigma_L(L = 180\,\mathrm{cm}) = (140 \pm 11)\,\mathrm{ps}.$$

By using different sets of laser runs, a systematic error of $\sim$15 ps, due to the system reproducibility, was estimated. This method eliminates all the contributions to the timing resolution which are common to both PMTs, including any jitter in the photodiode reference time.

Several systems, similar to this one, have achieved timing resolutions $\sim$100–200 ps. A selection is shown in Table 1 in order of increasing scintillator length L.

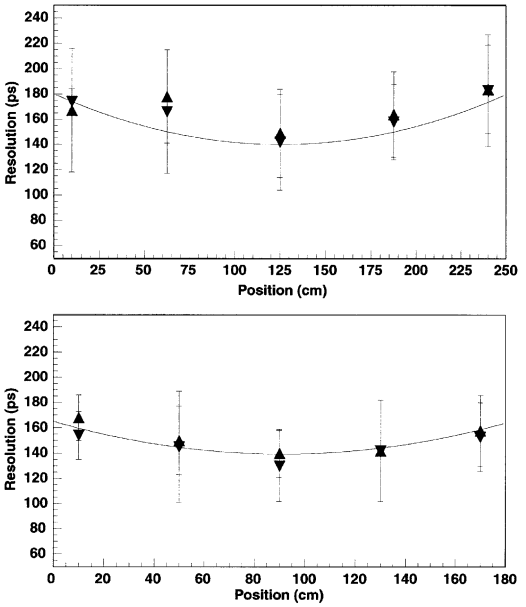

Fig. 8. Time resolutions σ_0^W as estimated from Eq. (5) (▼) and σ_0 from Eq. (4) (▲), after applying the correction for *time walk,* as a function of the distance from the left PMT along the counters with $L=250$ cm (above) and L=180 cm (below). The error bars show the rms of the distributions. The curve is shown to guide the eye.

4. Time calibration and monitoring during data taking

The initial timing calibration of the whole TOF detector (determination of the delay constants $\delta_{i,j}$ at time $T = T_0$) was done with a cosmic rays run in July 2001. Afterwards periodic recalibrations were taken with cosmic rays every 2–3 months during the HARP data taking, to re-determine the values of the calibration constants at fixed times. In between, the drift of these delays, as a function of the running time T, was traced by the laser calibration system.

4.1. Calibration with cosmic rays.

For the TOFW calibration about 3 million cosmic rays events were acquired during periods of 4 days in which the beam from the PS was off. The cosmic-ray trigger was based on the coincidence of both the corresponding calibration counters placed upstream and downstream the TOFW system (see Fig. 2). This resulted in an overall counting rate of ~25 Hz for the whole detector.

To properly evaluate the time-of-flight of the particles, the observed times of the PMT signals $\Delta t_{i,j}$ needed to be corrected for the time misalignment introduced by signal-cables, PMTs, discriminators, etc.:

$$\left(\Delta t^C\right)_{i,j} = \Delta t_{i,j} + \delta_{i,j} \tag{7}$$

where the $\delta_{i,j}$ offsets could be evaluated for each pair of PMTs of the ith scintillation counter as:

$$\delta_{i,1} = (\Delta t\_)_i + \Delta_i \delta_{i,2} = (\Delta t\_)_i + \Delta_i.$$

In eq. (8) the term $\Delta t_{-,i}$ corrects for the relative timing of the two PMTs for a center-crossing particle and is given by:

$$(\Delta t\_)_i = < \left(\frac{\Delta t_1 - \Delta t_2}{2}\right) i >. \tag{8}$$

The estimation of the second correction term, Δ_i, for the absolute timing with respect to the start counter (TOFA,TOFB or TDS), was more involved and was obtained with the following method.

The first step consisted in aligning in time the counters within each palisade by correcting for the time-of-flight between the ith counter and the reference counter placed downstream the TOFW:

$$\mathrm{TOF}_i = < \left(\frac{\Delta t_1 + \Delta t_2}{2}\right)_{\mathrm{REF}} - \left(\frac{\Delta t_{i,1} + \Delta t_{1,2}}{2}\right) >$$

by selecting the cosmic muons crossing the counters in their center with the same inclination $\theta \sim 40^\circ$. A time-walk correction (see Eq. (6)) was applied to TOF_i, improving the time-of-flight resolution by ~60 ps on average. The symmetry of the counter configuration does not require the evaluation of the cosmic muon's path which is virtually the same for each counter with respect to the reference.[13] In the central palisade this symmetry is fulfilled by requiring the coincidence of the counter of the TOFW with the corresponding one in the front strip and the 300 cm long downstream reference counter.

[13]The symmetry was reinforced by requiring a reconstructed longitudinal position in the reference counter, facing the hitted TOFW counter.

Table 1
Comparison of resolutions for several TOF detectors, based on plastic scintillators

Detector	Scint.	Length (cm)	Width (cm)	Thickness (cm)	PMT	σ (ps)
DIRAC [14]	BC420	40	7	2.2	Ham. R1828-01	123
NA49 [13]	BC408	12–48	1–1.25	1.5–2.4	Ham. R3478	80
DASP [15]	NE110	172	20	2	RCA 8575	210
E813 [16]	BC408	200	8.5	5	Ham. H1949	110
ARGUS [17]	NE110	218	9.3	2	RCA8575	~210
CLEOII [18]	BC408	280	10	5	XP2020	139
$N\bar{N}$ [8]	NE110	210–300	21	2	XP2020	~300
OBELIX [19]	NE110	300	9.3	4	XP2020	170
E735 [20]	BC408	305	10	5	XP2020	110
MARKIII [10]	NE Pilot F	317.5	15.6	5.1	XP2020	~170
DELPHI [21]	NE110	350	20	2	EMI19902KB	1200
CLAS [9]	BC408	32–450	15–22	5.1	XP43132B/D1	163
HARP	BC408	180–250	21	2.5	XP2020	~160

The three palisades were aligned with respect to each other using the particles crossing the overlap regions between the central and the lateral one[14] L-C-REF$_L$, and R-C-REF$_R$ (see Fig. 9):

$$\Delta t_{\mathrm{REF_L}} = \mathrm{TOF}(L - \mathrm{REF}_L) - \mathrm{TOF}(C - \mathrm{REF}_L)$$
$$\Delta t_{\mathrm{REF_R}} = \mathrm{TOF}(L - \mathrm{REF}_R) - \mathrm{TOF}(C - \mathrm{REF}_R). \quad (9)$$

Two global corrections were then introduced: c_1~150 ps to take into account the staggering of counters along the beam direction (~2.9 cm) and c_2~670 ps to take into account the shifted position of the left/right palisade with respect to the central one (~12.9 cm).

The absolute time calibration, with respect to the common start time t_s, was then achieved by adding the term $\mathrm{TOF}_{\beta=1}$, corresponding to the time-of-flight between the target and the TOFW of particles with $\beta = 1$, such as high momentum non-interacting pions from the beam. After the correction procedure, the quantities Δ_i are given by

$$\Delta_i = (\mathrm{TOF}_i + c_1) + (\Delta t_{\mathrm{REF}_{L,R}} + c_2) + \mathrm{TOF}_{\beta=1}. \quad (10)$$

Data analysis criteria were used to select single through-going muons traversing both the TOFW and the trigger counters, rejecting spurious events, such as showers, particles crossing the edge of the trigger counters, double hits in the same counter.

The overall distributions of the time-of-flight are shown in Fig. 10, taking the left wall as an example. The distributions obtained after the TOF_i alignment corrections and the time-walk correction confirm the effective time alignment of the three TOFW palisades. Assuming the same time resolution for the counters of the three walls and for the reference scintillators, the average intrinsic time resolution of the scintillators was σ_0~160 ps, in good agreement with the laboratory tests (see Section 3).

The three walls were then aligned in time by comparing the times-of-flight as described in Eq. (9). The precision on the time calibration constants was estimated to be ~60 ps, essentially dominated by the difference in angular acceptance introduced by the cosmic rays trigger for the counters at the edges of the left and right wall with respect to the counter at the center.

4.2. Time monitoring with the laser system.

The laser calibration system, previously described, was installed in HARP in May 2001 and operated continuously until the end of the experiment. The laser flash could be triggered externally, in the inter-spill, by a NIM level sent by a calibration trigger, so that data could be accumulated in dedicated runs or during the standard data-taking. For each PMT

[14]The same method can be used (with smaller statistical uncertainty) with the charged particles produced from the production target in physics runs.

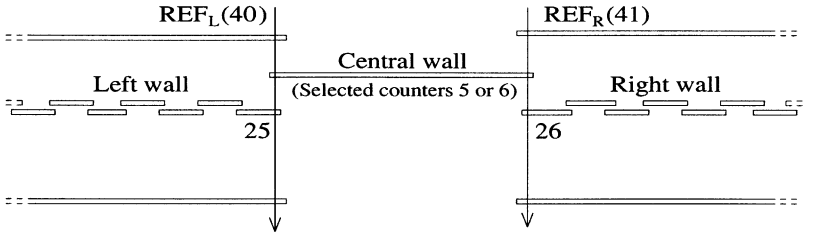

Fig. 9. The setup of the the three TOFW palisades and of the special cosmics counters (top view).

channel $j=1,2$ of a scintillation counter $i=1,\ldots 39$, data consisted of an ADC pulse-height $Q_{i,t}$ and a TDC information $\Delta t_{i,j}$. Time calibration of the TOFW system required the determination of the time-walk correction and of the relative time-offsets $\delta_{i,j}$ for each counter.

The time-walk corrections were determined both with cosmic rays and laser data. In the same ADC range results were in agreement. Using additional neutral density filters to vary the laser light injected into the fiber bundle, the pulse-height $Q_{i,j}$ and time differences $\Delta t_{i,j}$, from the start signal of the fast pin photodiode, were recorded for different laser intensities. Fig. 11 shows, for a typical PMT channel, the profile histogram of TDC times Δt as a function of the ADC pulse height Q. The behaviour of each individual channel was parameterized with the sum of an exponential and a low order polynomial function,[15] obtaining fit parameters for each individual channel. Signals compatible with a m.i.p had charge values around 100 pC and the settings of the laser calibration system were tuned to obtain values in this range for most channels. In some exceptional cases lower values were obtained, thus requiring a consistent time-walk correction.

The reliability of the time monitoring performed with the laser system was checked by comparing the variation of the counter time alignment constants δ_i obtained with cosmic rays calibration runs and laser calibration runs ($\Delta\delta_{CR}$ vs $\Delta\delta_L$). In order to correct for possible drifts of the pin-photodiode START signal, the laser constant variations were determined by subtracting the mean value $<\Delta\delta_L>$,

[15]This different functional form, with respect to cosmic rays data, was used to include in the fit also very low pulse height values ($Q\leqslant 30$ pC).

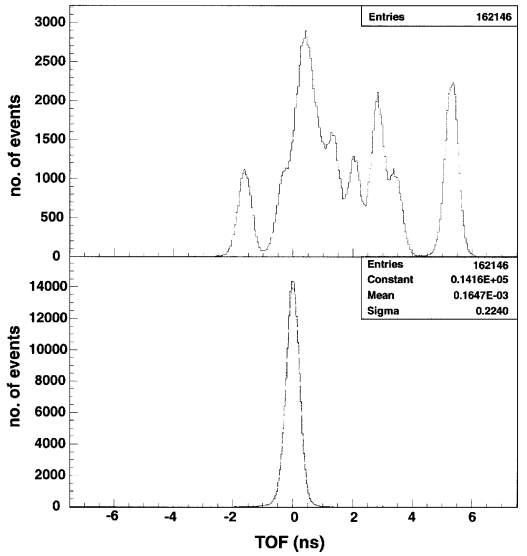

Fig. 10. Overall distribution of the time-of-flight for all the counters in the left palisade,without (top) and with (bottom) the time corrections described by Eq. (10).

averaged over all channels. Results from this comparison are reported in Fig. 12, showing that differences are well within a ± 100 ps band. Major interventions on the TOFW system were undertaken in May 2002 (change of PMTs HV), resulting in changes of the time calibration constants δ_i up to ± 0.5 ns, as measured with cosmic rays. This change was well followed by the laser system, as shown by Fig. 12. The root mean square (rms) of the difference between $\Delta\delta_{CR}$ and $\Delta\delta_L$; was around 40 ps, fully dominated by the laser system. As a consequence, a correction from laser data for time variations of the counters bigger than $\sim$70 ps could be safely applied.

The laser system could monitor the TOFW stability daily over all the data taking period. The

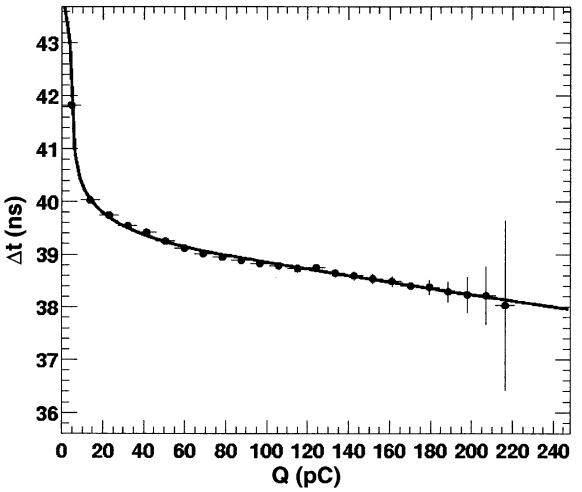

Fig. 11. Dependence of the TDC times (ns) vs. pulse height Q (pC) recorded in the ADC, for a typical PMT channel (no. 69). The fitted time-walk correction function $f(Q)$ is also shown.

TDC time differences $\Delta t_{i,j}$, measured at time T of the data taking period and corrected for time walk, have been studied for all PMT channels to monitor the long-term stability of the system. There was no evidence for time drift in excess of $\sim\pm 100$ ps over the full 2001 data taking period (3 months long). Fig. 13 shows the behaviour for the raw TDC / time difference $\Delta t_{i,j}$ for a typical channel, as a function of the running time T. From such trace plots, it was then possible to evaluate the evolution of the calibration constants $\delta_{i,j}$ for each PMT channel. Possible drifts in the calibration constants of the TOFW system due to temperature effects on a night–day timescale were also studied. No clear effects were seen, showing that the TOFW system was stable within the limits shown before. For the 2002 data taking, shifts in the electronics, due to a faulty discriminator board, were corrected for with the laser monitoring system. Apart these effects, results similar to the 2001 data taking were obtained for most of the running time.

5. First performance on beam.

The intrinsic counter resolution of the TOFW has been measured as $\sigma_0\sim 160$ ps. The resolution on the TOF measurement (σ_{TOF}) for particle identification in the forward region of the HARP experiment can be expressed as

$$\sigma_{\mathrm{TOF}} = \sqrt{\sigma_0^2 + \sigma_{t_s}^2 + \sigma_{\mathrm{calibr}}^2}$$

where σ_{t_s} is the resolution on the start signal (t_s) and σ_{calibr} (70 ps) is the resolution of the calibra-

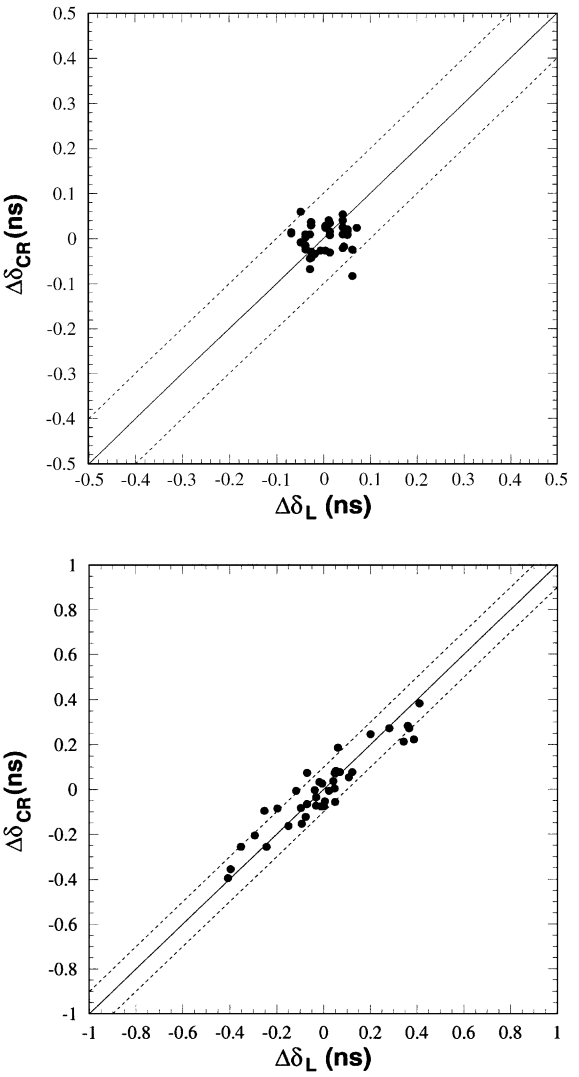

Fig. 12. $\Delta\delta_{\mathrm{CR}}$ are the drifts in the delay constants of each channel as measured with incoming cosmic ray muons at the beginning and the end of the 2001 August data taking period (a) and between May 2002 and November 2001 (b). $\Delta\delta_{\mathrm{L}}$ are the same drifts as measured with the laser system. The width of the dotted band in the plots is ± 70 ps.

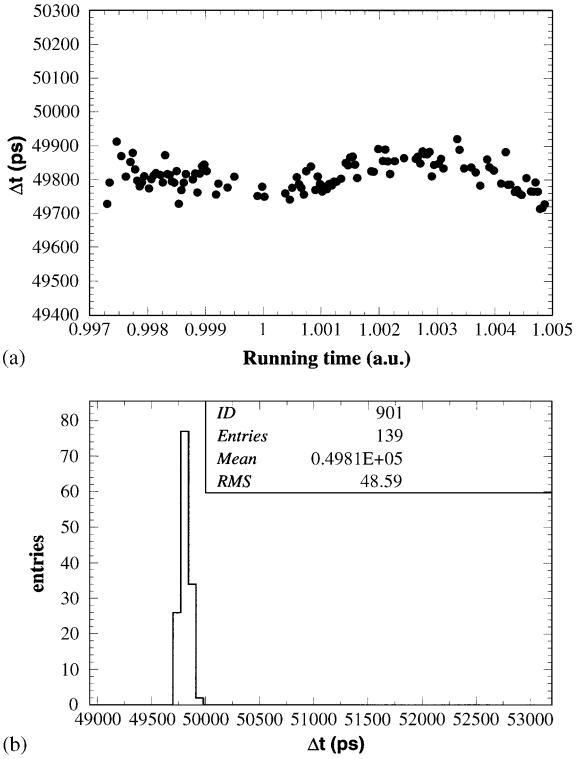

Fig. 13. (a) variation of the average time difference Δt vs running time T (2001 data taking: 3 months); (b) projected distribution of Δt: one entry for each laser calibration run (corresponding to individual dots of (a)) for a typical PMT channel (no. 60).

tion method used, over all the data taking period: that is including initial calibration of delays with cosmic rays (60 ps) and their time monitoring with the laser system (40 ps).

In the HARP experiment, the time-of-flight of particles produced at the target is obtained from the difference between the times measured in the TOFW and a start counter, such as TOFB, which has an intrinsic time resolution of about 100 ps. Therefore,the final time resolution on the TOF measurement is expected to be ~200 ps, considerably better than the design value of 250 ps.

5.1. Cross checks with the overlap method

A tool to cross-check the time equalization of the different scintillation counters is provided by the particles impinging on the overlap region of two adjacent slabs. Once the time responses of the slabs are aligned, and the scintillation counters' staggering along the particle trajectory is taken into account, the two counters should provide the same measurement of the particle's arrival time. This method can be applied to both beam particles and cosmic rays events.

The fit to the distribution of the difference in measured arrival time for two adjacent slabs also provides a measurement of the time resolution. The difference in crossing time for two adjacent slabs is compatible with $\Delta t = 0$ within the time alignment precision, which is ~100 ps given by the 70 s calibration precision for each counter (see Fig. 14). The corresponding measured time resolution

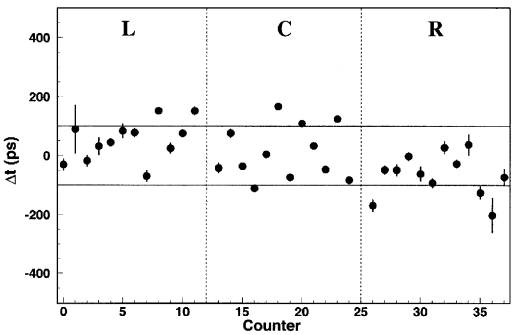

Fig. 14. Difference in crossing time for two nearby slabs, as a function of the first slab number for left, central and right palisades. The width of the dotted band in the plot is ± 100 ps, corresponding to the precision of the calibration method (1σ)). The low statistics of some points is due to a reduced geometrical acceptance.

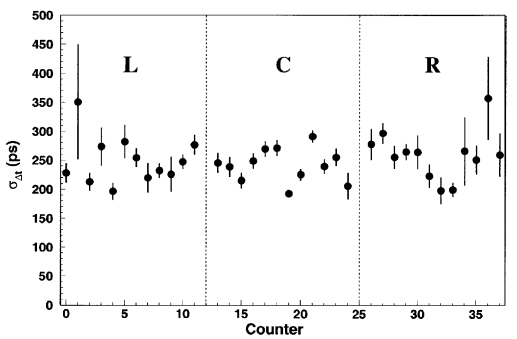

Fig. 15. Resolutions in ps for the overlap of two nearby slabs, as a function of the first slab number for left, central and right palisades.

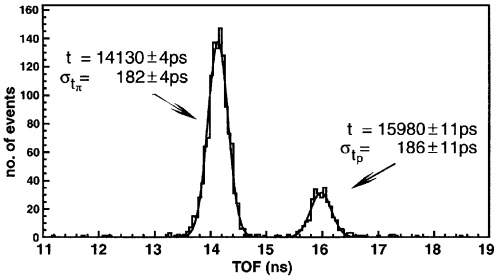

Fig. 16. Particle identification with the TOF detector, with 3 GeV incident unseparated hadron beam. The time-of-flight is computed between TOFB and the TOFW system. The pion and the proton peaks are clearly visible.

(~240 ps) is in good agreement with the expected value of ~230 ps, due to the ~160 ps intrinsic scintillation counter resolution, as shown in Fig. 15.

5.2. Particle identification

Particle identification in the HARP time-of-flight wall relies on the combination of particle momenta, as measured from the forward drift chambers, and the time of flight between a START signal (t_s) from a reference counter before the target and a STOP signal from the time-of-flight wall itself. The previous calibration issues are essential for the quality of the extracted TOF PID and thus the determination of particle masses. After the calibration procedure, π and p are separated at better than 7σ at 3 GeV/c, incident momentum, as shown in Fig. 16 for an empty target run. TOFW measurements have widths around 190 ps, as expected.

6. Conclusions

A large area TOF detector has been constructed for the HARP experiment at CERN PS. Individual counters have an intrinsic resolution of ~160 ps. Folding in calibrations and the contribution of the start detector a resolution of ~200 ps is obtained for the time of flight measurement of single particles. A π/p discrimination at better than 3σ is obtained up to 4 GeV/c of momentum.

Acknowledgements

We are greatly indebted to Ing. C. Arnaboldi and Mr. F. Chignoli, R. Mazza of INFN Milano and Mr. D. Filippi, P. Gesuato, D. Mazzaro and M. Turcato of INFN Padova for technical help in system preparation. We thank Prof. A. Pullia, INFN Milano, for his continuous support and the great help in the early stage of this project. We acknowledge also the contribution of Dr. M. Tagliaferri of Quanta Systems srl for the laser construction to the best of our specifications and Prof. D. Batani of INFM Milano for his generous help in many tests.

References

[1] M.G. Catanesi, et al., Proposal to study hadron production for the neutrino factory and for the atmospheric neutrino flux, CERN-SPSC/99-35, SPSC/P315, 15 November 1999;
A Cervera, HARP Collaboration, Status Report to SPSC, August 2003.
[2] M Apollonio, et al., Oscillation Physics with a Neutrino Factory, hep-ph/0210192, Geneva, October 2002.
[3] E. Church, et al., MiniBooNE Collaboration, Fermilab proposal P-0898, 1997.
[4] M.H. Ahn, et al., K2K Collaboration, Phys. Rev. Lett. 90 (2003) 021802.
[5] G. Prior, Nucl. Phys. Proc. Suppl B 125 (2003) 11;
M. Bogomilov, Nucl. Instr. Meth. A508 (2003) 152.
[6] M. Anfreville, et al., NIM A 481 (2002) 339.
[7] K. Pretzl, et al., Invited talk at the International Symposium on Strangeness and Quark Matter, Crete, 1999, p. 230.
[8] M. Baldo Ceolin, et al., Nuovo Cimento 105A (1992) 1679.
[9] J.S. Brown, et al., Nucl. Instr. and Meth. 221 (1984) 503.
[10] E.S. Smith, et al., Nucl. Instr. and Meth A 432 (1999) 265.
[11] T. Kishida, et al., Nucl. Instr. and Meth A 254 (1987) 367.
[12] M. Bonesini, et al., IEEE Trans. Nucl. Sci NS-50 (4) (2003) 1053.
[13] G. Palla, et al., Nucl. Instr. and Meth. A 451 (2000) 406.
[14] B. Adeva, et al., Nucl. Instr. and Meth A 491 (2002) 41.
[15] W. Braunschweig, et al., Nucl. Instr. and Meth. 134 (1976) 261.
[16] V. Sum, et al., Nucl. Instr. and Meth. A 326 (1993) 489.
[17] R. Heller, et al., Nucl. Instr. and Meth. A 235 (1985) 26.
[18] Y. Kubota, et al., Nucl. Instr. and Meth. A 320 (1992) 66.
[19] G.C. Bonazzola, et al., Nucl. Instr. and Meth. A 356 (1995) 270.
[20] S. Benerjee, et al., Nucl. Instr. and Meth. A 269 (1988) 121.
[21] J.M. Bennloch, et al., Nucl. Instr. and Meth. A 292 (1990) 319.